

Size and Shape Control of Monodisperse FePt Nanoparticles

Vikas Nandwana, Kevin E. Elkins, Narayan Poudyal, Girija S. Chaubey, Kazuaki Yano, and J. Ping Liu*

Department of Physics, University of Texas at Arlington, Arlington, Texas 76019

Received: December 4, 2006; In Final Form: January 17, 2007

Morphological control of FePt nanoparticles has been systematically studied. By varying synthetic parameters including precursors, solvents, amount of surfactants, and heating rate of the solution, the particle size from 2 to 9 nm can be tuned with 1 nm accuracy. While most particles are spherical in shape, cubic particles can be obtained when particles are greater than 7 nm. Rod-shape nanoparticles have also been obtained. The as-synthesized nanoparticles are found to be superparamagnetic at room temperature and their blocking temperature is size dependent that increases with particle size. After annealing in a reducing atmosphere, the nanoparticles form hard magnetic films with ordered fct structure and high coercivity up to 2.7 T.

Introduction

There has been renewed research interest in monodisperse magnetic nanoparticles in recent years, driven by new applications such as ultrahigh-density magnetic storage media,¹ biological imaging and therapy,² and exchange-coupled nanocomposite magnets.³ Recently, various magnetic nanoparticles including FePt,⁴ Co,⁵ CoPt,⁶ and Fe₃O₄⁷ have been fabricated by solution-phase synthesis. Preparation of high quality nanoparticles with desired size and shape is a prerequisite to investigate and utilize their properties. Relatively simple and reproducible approaches for the synthesis of crystalline nanoparticles of controllable size are of great fundamental and technological interest. The control of the nanocrystal size and shape is also a key in the formation of two or three-dimensional self-assembled structures where individual nanocrystals are the building blocks of the next level of material hierarchy.⁸

Although many factors affect particle size and shape of nanoparticles during chemical synthesis, only few parameters have been studied for FePt system. Recently, size control of monodisperse FePt nanoparticles from organometallic precursors and microemulsion was reported.^{9,10} It was found that separation of nucleation and growth in time is required for the formation of particles with a near-monodisperse size distribution.¹¹ However, fine tuning of the particle size remains a challenging task. Here, we report our effort in FePt particle size control with 1 nm accuracy by changing several synthetic parameters.

Experimental Methods

FePt nanoparticles were prepared via chemical reduction of Pt(acac)₂ and thermal decomposition of Fe(CO)₅ in the presence of oleic acid and oleyl amine. The synthetic experiments were carried out using standard airless technique in argon atmosphere. In a typical procedure, 0.5 mmol of platinum acetylacetonate was added to 125 mL flask containing a magnetic stir bar and mixed with 20 mL of octyl/benzyl ether. After purging with argon for 30 min at room temperature, the flask was heated up to 120 °C for 10 min and a designated amount of oleic acid and oleyl amine was added. Iron pentacarbonyl or iron acetylacetonate were used as an iron precursor. Iron acetylacetonate (0.5 mmol) was added at room temperature while iron pentacarbonyl (1.0 mmol) was added at 120 °C when the platinum precursor dissolved completely. The dissolution of Pt(acac)₂ in solvent could be followed experimentally by the change of color of the solution from off yellow to transparent yellow. After the addition of Fe(CO)₅, the color transition from golden to black suggested formation of nanoparticles in the solution. Then it was heated to 298 °C for 1 h before cooling to room temperature under the argon blanket. Argon gas was flowed throughout the experiment. The heating rate was varied from 1 to 15 °C per minute according to the experimental design.

The black product was precipitated by adding ethanol and separated by centrifugation and redispersed in hexane. To achieve the highest purity, extra ethanol was added in this dispersion and the dispersion was centrifuged again. Because all the particles were quite homogeneous, size selection was not necessary. After washing the particles in ethanol three or more times, they were dispersed in hexane and stored in glass bottles under refrigeration. Samples for magnetic characterization were prepared by depositing a drop of the final hexane dispersion on a 3 × 3 mm silicon substrate, evaporating the solvent at room temperature and further drying in vacuum, which led to the formation of FePt nanoparticle-assembled thin films. The samples were then annealed at 650 °C for 1 h under the flow of forming gas (Ar + 7% H₂) in a tube furnace.

The transmission electron microscopy (TEM) images were recorded on a JEOL 1200 EX electron microscope at an accelerating voltage of 120 kV. Powder X-ray diffraction (XRD) spectra were recorded on a Philips MPD diffractometer with a Cu K α X-ray source ($\lambda = 1.5405 \text{ \AA}$). The magnetic hysteresis measurements have been carried out by using superconducting quantum interference device (SQUID) magnetometer with magnetic field up to 7 T. The composition analysis was done by energy dispersive X-ray spectroscopy (EDX) and inductively coupled plasma (ICP).

The transmission electron microscopy (TEM) images were recorded on a JEOL 1200 EX electron microscope at an accelerating voltage of 120 kV. Powder X-ray diffraction (XRD) spectra were recorded on a Philips MPD diffractometer with a Cu K α X-ray source ($\lambda = 1.5405 \text{ \AA}$). The magnetic hysteresis measurements have been carried out by using superconducting quantum interference device (SQUID) magnetometer with magnetic field up to 7 T. The composition analysis was done by energy dispersive X-ray spectroscopy (EDX) and inductively coupled plasma (ICP).

Results and Discussions

We examined several parameters that have an effect on the size and shape of monodisperse FePt nanoparticles. After examining each parameter thoroughly, we found that surfactants

* Corresponding author. E-mail: pliu@uta.edu. Tel: +1-817-272-2815. Fax: +1-817-272-3637.

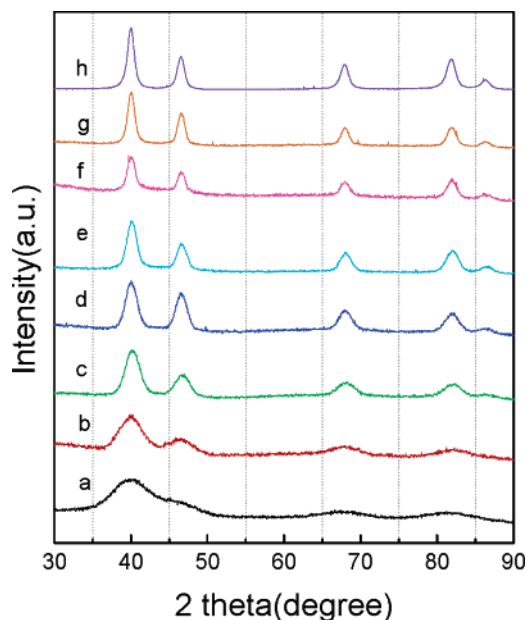


Figure 1. XRD curves of as-synthesized FePt nanoparticles of size (a) 2 nm, (b) 3 nm, (c) 4 nm, (d) 5 nm, (e) 6 nm, (f) 7 nm, (g) 8 nm, and (h) 9 nm.

and their concentration, type of solvents, nature of precursors, and heating rate are the key parameters which play a crucial role in size and shape control of the nanoparticles.

Size Control. Figure 1 shows XRD patterns of as-synthesized FePt nanoparticles of 2 to 9 nm with 1 nm difference. It can be seen that the peak width decreases as the particle size increases. We can also see from the figure that these particles exhibit a face-centered cubic (fcc) crystal structure. The average particle diameter estimated from Scherrer's formula¹² for each curve in Figure 1 is the same with that determined by statistical analysis of the TEM images (Figure 2) with $\pm 10\%$ difference. It is obvious that each individual particle is a single crystal.

The formation mechanism of FePt nanoparticles is similar as previously reported.⁹ At the early stage of the synthesis, Pt-rich nuclei are formed from the reduction of Pt(acac)₂ and the slow decomposition of Fe(CO)₅. More Fe atoms then diffuse into existing Pt-rich nuclei until complete decomposition of Fe(CO)₅. The amount of Fe diffusing into Pt-rich nuclei relates to the surface area of the latter. The size of the Pt-rich nuclei is dependent on the nucleation rate, which can be controlled by varying the reaction parameters. Smaller Pt-rich nuclei have a greater surface specific area compared to the larger Pt-rich nuclei; the diffusion of Fe will make the composition of the smaller nuclei richer in Fe as opposed to the larger nuclei resulting in larger FePt nanoparticles with higher Pt content. Refluxing the reaction mixture above 295 °C leads to complete atomic diffusion and formation of fcc FePt nanoparticles.

Surfactants typically play a crucial role in controlling the size and shape of chemically synthesized nanoparticles. Oleic acid and oleyl amine were chosen in our synthesis as they work as ideal ligands for FePt nanoparticles. We examined the effect of the surfactants to Pt(acac)₂ molar ratio to observe the size of monodisperse FePt nanoparticles. The heating rate of the reaction was maintained at 5 °C/min. FePt nanoparticles with average size of 4 nm (Figure 2(c)) were obtained when the molar ratio of surfactants to Pt(acac)₂ was 1. By decreasing the molar ratio to 0.75, the particle size decreased to 3 nm (Figure 2(b)) whereas by increasing the molar ratio up to 10, the particle size increased to 9 nm (Figure 2(h)). It is clear that the particle size increases with increasing surfactant concentration¹⁰ but after a

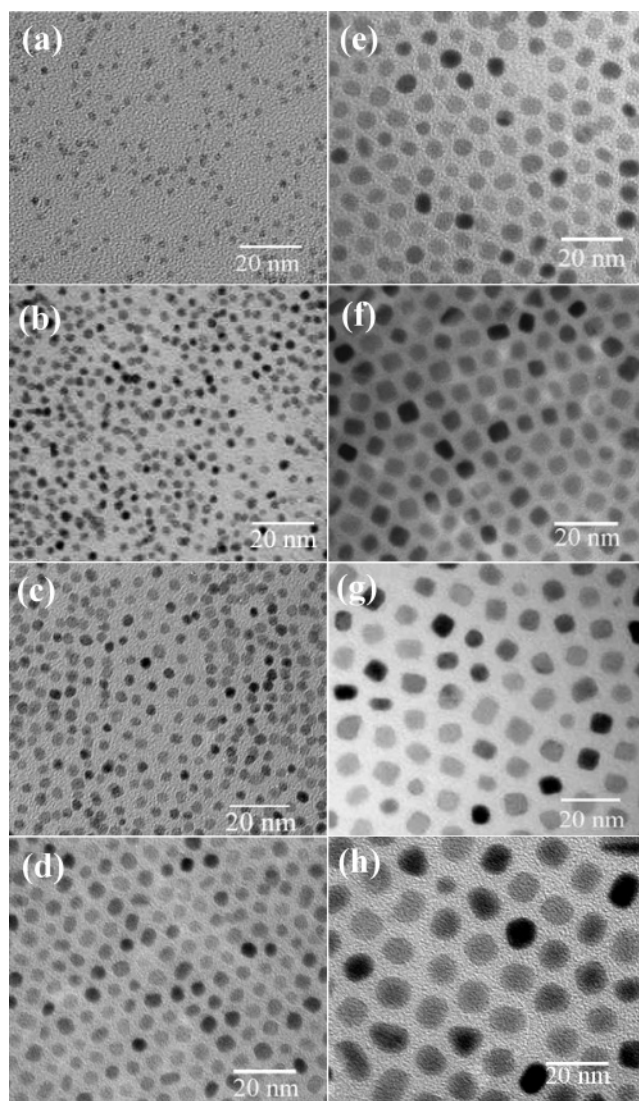


Figure 2. TEM image of as-synthesized FePt nanoparticles of size (a) 2 nm, (b) 3 nm, (c) 4 nm, (d) 5 nm, (e) 6 nm, (f) 7 nm, (g) 8 nm, and (h) 9 nm.

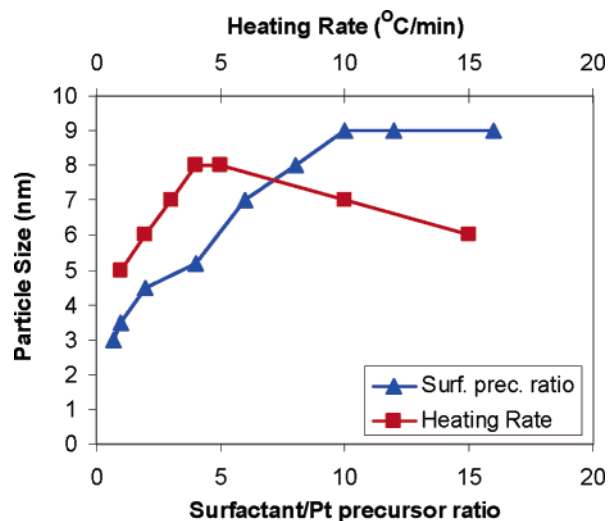


Figure 3. Heating rate and surfactant/Pt precursor dependence on particle size.

certain concentration of surfactants the size did not change (Figure 3). The resultant size change of the nanoparticles is thought to be the result of the change in the number of nuclei

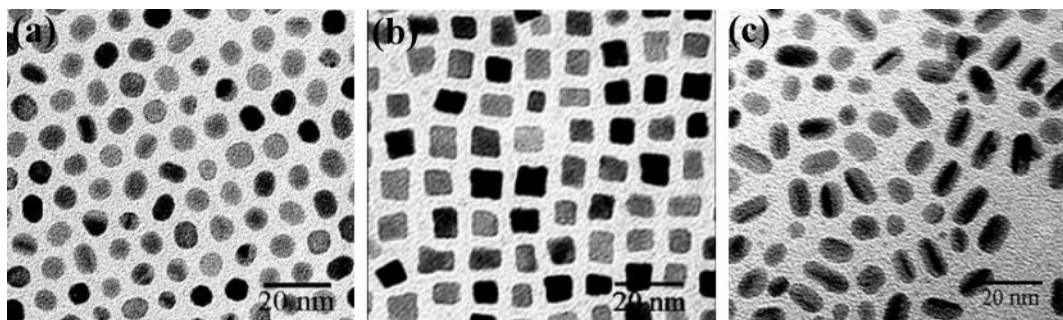


Figure 4. TEM image of (a) spherical, (b) cubic, and (c) rod-shape FePt nanoparticles.

at the first step of particle formation. It is believed that the increase in the surfactant amount resulted in the formation of stable complexes with individual metal atoms of a molecular precursor. Therefore, an increase in surfactant concentration is expected to suppress the nucleation process and as a consequence, larger particle size is produced.

The heating rate of reaction mixture was also found to be very important in the fine-tuning of the particle size. To analyze the size change with the heating rate of the reaction mixture, surfactant to precursor ratio identical to that used to synthesize 8 nm particles (Figure 2(g)) was chosen. As the heating rate was increased from 5 to 10 and then to 15 °C/min, we found that the average particle size was decreased from 8 to 7 and then to 6 nm (Figure 2(f) and 2(e)), respectively. With the increase in the heating rate, the nucleation rate was increased. As a result of the enhanced nucleation rate, more nuclei were formed at the initial stage. Consequently smaller particles were produced. On the other hand, the correlation between the heating rate and the particle size is not always monotonous. When the heating rate is very low, competition between the nucleation and the growth occurs and smaller particles may be produced. For example, when the heating rate was decreased to 1 °C/min, surprisingly the particle size was decreased to 5 nm. Our results suggest that nucleation rate dominates over growth rate at a very low heating rate. This competition arises due to several parameters including precursors. $\text{Fe}(\text{CO})_5$ was used as the iron source to synthesize particles from 3 to 9 nm. However, particle size below 3 nm was not obtained using $\text{Fe}(\text{CO})_5$. To study the effect of precursors on the particles size, $\text{Fe}(\text{CO})_5$ was replaced by $\text{Fe}(\text{acac})_3$, while keeping all the synthetic conditions same. When $\text{Fe}(\text{acac})_3$ was used, the particles of 2 nm were obtained (Figure 2(a)). The nature of the precursor and their physical state are believed to be the reason for the decrease in particle size. $\text{Fe}(\text{CO})_5$ is a volatile liquid and was injected to the reaction mixture after dissolution of $\text{Pt}(\text{acac})_2$ in octyl ether. In comparison, $\text{Fe}(\text{acac})_3$ is a solid powder that was mixed with $\text{Pt}(\text{acac})_2$ in octyl ether at room temperature. The reason for such small size may be a quick nucleation from precursor decomposition followed by an immediate precursor depletion. The nucleation rate dominates over growth rate, and the abundance of nuclei with less growth leads to the formation of the 2 nm particles. The details of the mechanism have been given in our previous paper.¹³ The interesting point was that although the amount of surfactant and heating rate were varied, particle size was always found to be 2 nm when $\text{Fe}(\text{acac})_3$ was used as the iron precursor. As reported previously, heating rate did not cause significant change in particle size when iron(III) ethoxide [$\text{Fe}(\text{OEt})_3$] was used as iron source.^{10b} Efforts are being made to synthesize larger than 9 nm and success has been achieved to produce 15 nm FePt nanoparticles.

Shape Control. Solvents provide the media for particles to nucleate and grow. The correct composition of Fe and Pt is required to form the desired phase. A solvent with high boiling point and chemical stability at higher temperature is required to achieve the correct composition of FePt by interatomic diffusion. Because of its stability at reflux temperature (295 °C), octyl ether is a most commonly used solvent for FePt nanoparticle synthesis. However, octyl ether is a very expensive solvent; therefore benzyl ether was used as an alternative solvent for most of the experiments. When benzyl ether was used as solvent, monodisperse spherical particles with narrow size distribution were obtained. Nevertheless, while using benzyl ether it was very difficult to maintain the reflux temperature as it releases some low-boiling point byproducts at high temperature (above 280 °C) that results in the lowered temperature of the reaction mixture. Therefore, to maintain correct composition, octyl ether was used in our experiments. Interestingly, faceted cubic shape (Figure 4(b)) FePt nanoparticles instead of the spherical ones (Figure 4(a)) were obtained when octyl ether was used as the solvent. The change in shape of the nanoparticles could be related to the molecular structure of the solvents. Ether group molecules are attached inbetween two benzene rings in benzyl ether whereas octyl ether has a linear structure with the ether group attached to both sides by hydrocarbon chain, which could have served as the matrix for the resultant shape. However, this shape change was only observed in particles larger than 7 nm but was hard to find in the smaller particles.

The time interval of surfactant injection into the reaction mixture is another factor that influences the particle shape. In our synthesis procedure, both of the surfactants were injected simultaneously a few seconds after the injection of $\text{Fe}(\text{CO})_5$. However, when using benzyl ether as a solvent, when oleyl amine was injected after 5 min of injection of oleic acid, rod shape nanoparticles (Figure 4(c)) with few spherical ones were obtained. The same result was not observed when octyl ether was used as the solvent. The mechanism of rod formation has not been well understood at this stage. This is an interesting finding because rod shape nanoparticles are good candidates for anisotropic nanomagnets as they may be aligned by virtue of their shape.

Composition Control and Magnetic Properties. The as-synthesized FePt nanoparticles have chemically disordered fcc structure with low-magnetic anisotropy. Magnetic properties of the as-synthesized FePt nanoparticles were measured by SQUID. Figure 5 shows the hysteresis loops of as-synthesized FePt particles of 2, 4, and 8 nm. It has been found that all the nanoparticles are superparamagnetic at 300 K. This indicates that the thermal energy can overcome the anisotropy energy barrier of the individual particles, and the net magnetization of these nanoparticle assemblies is zero in the absence of an

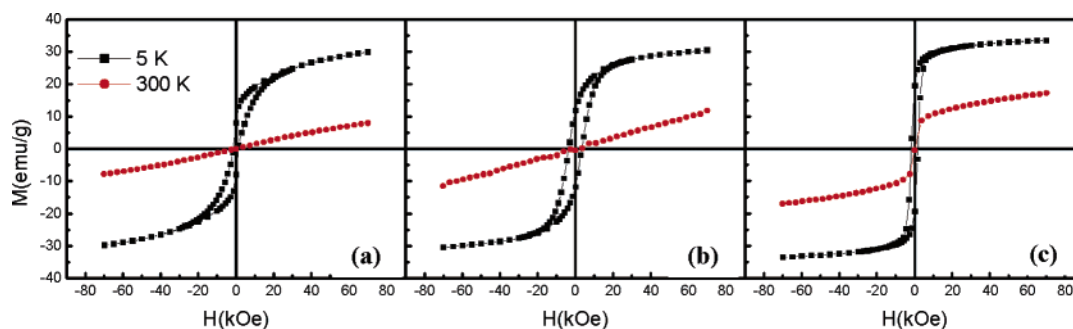


Figure 5. Hysteresis loops of the (a) 2 nm, (b) 4 nm, and (c) 8 nm FePt nanoparticle assemblies measured at 5 and 300 K.

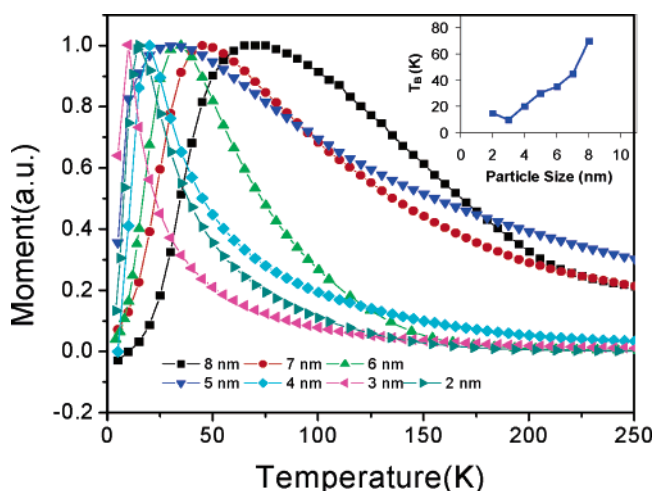


Figure 6. Magnetization versus temperature for 2 to 8 nm FePt nanoparticles measured at 100 Oe field.

external field. However all the particles are ferromagnetic at 5 K and magnetization is much higher compared to that at 300 K (Figure 5). It is also observed that the saturation magnetization values of the particles are size dependent and increase with particle diameters.

The temperature dependence of magnetization of different size particles was measured with zero-field cooling (ZFC) and field cooling (FC) procedures. On cooling, the ZFC magnetization begins to drop and deviate from FC magnetization at blocking temperature T_B . Figure 6 shows the plot of magnetization (M) versus temperature (T) for 2, 3, 4, 5, 6, 7, and 8 nm FePt nanoparticles with a measuring field of 100 Oe between 5 and 250 K. The M versus T curves show peaks characteristic of superparamagnetic transitions. The peak temperature in the M versus T curve (blocking temperature T_B) increases continuously with the increasing particle size (Figure 6); for example, the T_B values for 2, 5, and 8 nm particles are 15, 30, and 70 K, respectively.

The magnetic properties of these particles strongly depend on their composition. The composition of the as-synthesized FePt nanoparticles was determined by EDX and ICP. The average compositions of 2, 4, 6, 8, and 9 nm FePt particles were found to be $\text{Fe}_{54}\text{Pt}_{46}$, $\text{Fe}_{52}\text{Pt}_{48}$, $\text{Fe}_{48}\text{Pt}_{52}$, $\text{Fe}_{46}\text{Pt}_{54}$, and $\text{Fe}_{45}\text{Pt}_{55}$, respectively. It was observed that with increasing particle size there was a slight increase in Pt content.⁹ However, the synthesized FePt particles have the single-phase structure after annealing (the equal atomic L1_0 phase) and the composition fluctuation has been under control.

The as-synthesized disordered fcc structure FePt nanoparticles with low magnetic anisotropy can be transformed into fct structure with very high magnetic anisotropy through thermal

annealing. These fcc particles were deposited on an Si substrate and were annealed in forming gas (Ar + 7% H_2) at 650 °C for 1 h. In equal atomic FePt phase, magnetic hardening shown by the coercivity is based on the fcc–fct phase transition.¹⁴ After the annealing, all the particles gave a coercivity of more than 1.5 T, and the highest coercivity achieved was 2.7 T in the 2 nm particles. The very high coercivity indicates the complete phase transformation of these nanoparticles and also shows that the particles are a single phase material, which is consistent with the XRD results.

Conclusions

High quality FePt nanoparticles of 2 to 9 nm in size with narrow size distribution have been prepared in a predictable and reproducible manner via chemical solution methods. The size and shape of these particles can be controlled in a systematic manner. The FePt nanoparticle size increases with increasing concentration of surfactants (oleic acid, oleyl amine). This effect attributes to the slow rate of nucleation at a high concentration of the stabilizer. The average size of nanoparticles changes with changing heating rate also. The shape of the nanoparticles is found to be influenced by solvent types and by the time interval of injection of surfactants. The as-synthesized nanoparticles were found to be superparamagnetic at room temperature and their blocking temperature is size dependent, which increases with particle size. After annealing in a reducing environment, thin film assemblies of these nanoparticles give coercivity up to 2.7 T, which indicates their complete transformation from the disordered fcc to the ordered fct structure.

Acknowledgment. This work was supported by ONR/MURI under the Grant No. N00014-05-1-0497 and DoD/DARPA through ARO under Grant No. DAAD 19-03-1-0038.

References and Notes

- (1) (a) Sun, S. H.; Murray, C. B.; Weller, D.; Folks, L.; Moser, A. *Science* **2000**, *287*, 1989–1992. (b) Weller, D.; Doerner, M. F. *Annu. Rev. Mater. Sci.* **2000**, *30*, 611–644.
- (2) (a) Hafeli, U.; Schutt, W.; Teller, J.; Zborowski, M. *Scientific and Clinical Applications of Magnetic Carriers*; Plenum Press: New York, 1997. (b) Safarik, I.; Safarikova, M. *Monatsh. Chem.* **2002**, *133*, 737–759. (c) Perez, J. M.; O’Loughin, T.; Simeone, F. J.; Weissleder, R.; Josephson, L. *J. Am. Chem. Soc.* **2002**, *124*, 2856–2857. (d) Pouliquen, D.; Chouly, C. *Magnetic Microcarriers for Medical Applications*; Arshady, R., ed.; Citus Books: London, 1999; pp 343–382. (e) Zhao, M.; Josephson, L.; Tang, Y.; Weissleder, R. *Angew. Chem. Int. Ed.* **2003**, *42*, 1375–1378.
- (3) Zeng, H.; Li, J.; Liu, J. P.; Wang, Z. L.; Sun, S. H. *Nature* **2002**, *420*, 395–398.
- (4) (a) Sun, S.; Fullerton, E. E.; Weller, D.; Murray C. B. *IEEE Trans. Magn.* **2001**, *37* (4), 1239–1243. (b) Jeyadevan, B.; Hobo, A.; Urakawa, K.; Chinnasamy, C. N.; Shinoda, K.; Tohji, K. *J. Appl. Phys.* **2003**, *93*, 7574–7576.
- (5) (a) Sun, S.; Murray, C. B. *J. Appl. Phys.* **1999**, *85*, 4325–4330. (b) Petit, C.; Taleb, A.; Pileni, M. P. *J. Phys. Chem. B* **1999**, *103*, 1805–

1810. (c) Puentes, V. F.; Krishnan, K. M.; Alivisatos, A. P. *Science* **2001**, *291*, 2115–2117.

(6) (a) Park, J. I.; Cheon, J. *J. Am. Chem. Soc.* **2001**, *123*, 5743–5746. (b) Chen, M.; Nikles, D. E. *J. Appl. Phys.* **2002**, *91*, 8477–8479. (c) Chinnasamy, C. N.; Jeyadevan, B.; Shinoda, K.; Tohji, K. *J. Appl. Phys.* **2003**, *93*, 7583–7585.

(7) (a) Sapiaszko, R. S.; Matijevic, E. *J. Colloid Interface Sci.* **1980**, *74*, 405–407. (b) Kang, Y. S.; Risbud, S.; Rabolt, J. F.; Stroeve, P. *Chem. Mater.* **1996**, *8*, 2209–2211. (c) Hong, C. Y.; Jang, I. J.; Horng, H. E.; Hsu, C. J.; Yao, Y. D.; Yang, H. C. *J. Appl. Phys.* **1997**, *81*, 4275–4277. (d) Vijayakumar, R.; Koltypin, Y.; Felner, I.; Gedanken, A. *Mater. Sci. Eng., A* **2000**, *286*, 101–104. (e) Fried, T.; Shemer, G.; Markovich, G. *Adv. Mater.* **2001**, *13*, 1158–1161. (f) Sun, S.; Zeng, H. *J. Am. Chem. Soc.* **2002**, *124*, 8204–8205.

(8) (a) Murray, C. B.; Kagan, C. R.; Bawendi, M. G. *Annu. Rev. Mater. Sci.* **2000**, *30*, 545–548. (b) Murray, C. B.; Kagan, C. R.; Bawendi, M. G. *Science* **1995**, *270*, 1335–1338. (c) Rogach, A. L.; Talapin, D. V.; Shevchenko, E. V.; Kornowski, A.; Haase, M.; Weller, H. *Adv. Funct. Mater.* **2002**, *12*, 653–664. (d) Collier, C. P.; Vossmeier, T.; Heath, J. R. *Annu. Rev. Phys. Chem.* **1998**, *49*, 371–374.

(9) (a) Chen, M.; Liu, J. P.; Sun, S. *J. Am. Chem. Soc.* **2004**, *126*, 8394–8395. (b) Yan, Q.; Purkayastha, A.; Kim, T.; Kröger, R.; Bose, A.; Ramanath, G. *Adv. Mater.* **2006**, *18* (19), 2569–2573. (c) Nakaya, M.; Kanehara, M.; Teranishi, T. *Langmuir* **2006**, *22*, 3485–3487.

(10) (a) Momose, S.; Kodama, H.; Uzumaki, T.; Tanaka, A. *Jpn. J. Appl. Phys.* **2005**, *44*, 1147–1149. (b) Saita, S.; Maenosono, S. *Chem. Mater.* **2005**, *17*, 6624–6634.

(11) Watzky, M. A.; Finke, R. G. *J. Am. Chem. Soc.* **1997**, *119*, 10382–10400.

(12) Cullity, B. D. *Introduction to Magnetic Materials*; Addison-Wiley: London, 1972.

(13) Nandwana, V.; Elkins, K. E.; Liu, J. P. *Nanotechnology* **2005**, *16*, 2823–2826.

(14) (a) Elkins, K. E.; Li, D.; Poudyal, N.; Nandwana, V.; Jin, Z.; Chen, K.; Liu, J. P. *J. Phys. D: Appl. Phys.* **2005**, *38*, 2306–2309. (b) Li, D.; Poudyal, N.; Nandwana, V.; Jin, Z.; Elkins, K. E.; Liu, J. P. *J. Appl. Phys.* **2006**, *99*, 08E911. (c) Liu, J. P.; Elkins, K. E.; Li, D.; Nandwana, V.; Poudyal, N. *IEEE Trans. Magn.* **2006**, *42*, 3036–3041. (d) Rong, C. B.; Li, D.; Nandwana, V.; Poudyal, N.; Elkins, K. E.; Liu, J. P. *Adv. Mater.* **2006**, *18*, 2984–2988.